Compaction process in concrete during missile impact: a DEM analysis

Wenjie SHIU*, Frédéric-Victor DONZÉ, Laurent DAUDEVILLE

Laboratoire "Sols Solides Structures et Risques", UMR5521, Université Joseph Fourier, Grenoble Université ,

BP53, 38041 GRENOBLE cedex 9, FRANCE

*Corresponding author: wen-jie.shiu@hmg.inpg.fr Tel. +33 (0)4 76 82 70 04

Fax. +33 (0)4 56 52 86 42

Abstract: A local behavior law, which includes elasticity, plasticity and damage, is developed in a three dimensional numerical model for concrete. The model is based on the Discrete Element Method (DEM) and the computational implementation has been carried out in the numerical Code YADE. This model was used to study the response of a concrete slab impacted by a rigid missile, and focuses on the extension of the compacted zone. To do so, the model was first used to simulate compression and hydrostatic tests. Once the local parameters were calibrated, the numerical model simulated the impact of a rigid missile used as a reference case to be compared to an experimental data set. From this reference case, two additional simulations were carried out: first, with a different impact velocity and second, a different ratio between the thickness of the target and the diameter of the missile. The results show the importance of compaction during an impact and how it expands depending on the impact parameters.

Keywords: Impact missile, concrete model, Discrete Element Method;

1 INTRODUCTION

When a reinforced concrete structure is impacted, the material is subjected to various states of stress. Near the impactor, the state of stress produces irreversible compaction, whereas farther from this location, the material experiences compression with a moderate triaxial stress state (Burlion et al., 2000). Moreover, in case of a thin concrete target, the compressive wave reflection results in a tensile wave and can produce scabbing (Magnier & Donze, 1998). The computational analysis of reinforced concrete walls subjected to this type of loading history must be capable of capturing the key features of the material response under such loads: tensile cracking, compression failure, the effect of confinement on the ultimate stress and compaction.

The Discrete Element Method (DEM) (Cundall and Strack, 1979), which is an alternative numerical method to continuum-type methods, is used here to study the behavior of concrete structures subjected to rigid impacts. This method does not rely upon any assumption about where and how a crack or several cracks occur and propagate, since the medium is naturally discontinuous and is very well adapted to dynamic problems, when a transition from the solid state to a granular flow regime is observed. However, using solely local elastic-brittle or even elastic-perfectly plastic constitutive laws are not sufficient to reproduce quantitatively the behavior of the concrete material (Hentz et al., 2004a). In this work, an attempt was made to develop a local elastic-bilinear hardening-damage constitutive law in order to capture the local compaction process which can not be taken into account intrinsically, when using a dense packing of non-deformable discrete elements. The constitutive parameter values were set here using a series of compressive experiment tests on concrete, which were carried out with a high confinement triaxial cell (Gabet et al., 2007). The maximum

confining pressure is about 1 GPa which is close to the maximum pressure which can be expected in the impacted area.

After presenting the numerical model in section 1, the local parameter identification process is given in section 2. This model is then applied to simulate the impact of a rigid missile on a reinforced concrete slab. This configuration is based on the experimental CEA-EDF tests (Berriaud et al., 1978). Section 3 deals with the numerical simulations of the impact test. The result for the reference case was compared with the results of a previous DEM model (Shiu et al., 2007a) which used a simple local elastic-brittle model. Then, using the same local parameters in the numerical model, additional simulations were performed to study the evolution of the compacted zone.

2 THE DEM MODEL

The discrete element method is used in this work to study the behavior of concrete under strict dynamic loading. The numerical tests were simulated with an open DEM code, YADE (Kozicki and Donzé, 2007, YADE, 2004). Note that YADE is a code based on the Discrete Element Method, using a force-displacement approach (see Eq. (1.a)), Newton's second law of motion, Eq. (1.b) and Eq. (1.c), describes the motion of each element as the sum of all forces applied on this element. The dynamic behavior of the system is solved numerically by a time algorithm in which the velocities and the accelerations are constant at each time step. The system evolves and an explicit finite difference algorithm is used to reproduce this evolution.

The equations of motion applied to each element are defined by.

$$F_i = K_i U_i \qquad , \qquad (1.a)$$

$$F_i = m(\ddot{x}_i - g_i) \qquad \text{(Translational motion)} \quad , \qquad (1.b)$$

4

$$M_i = I\,\dot{\omega}_i \qquad \text{(Rotational motion)} \quad , \qquad (1.c)$$

where F_i is the ith component of the contact force, K_i is the stiffness associated to each element, with K_n in the normal direction and K_s in the tangent direction, U_i is the overlap between two elements in contact, m is the mass of each element, $\ddot{x}_i$ and $\dot{\omega}$ are the translational acceleration and rotational acceleration respectively, g_i is the gravitational acceleration, M_i is the resultant moment acting on each element and I is the moment of inertia. During the calculation cycle, the force-displacement law (eq.(1.a)) is calculated first, then the new element's position will be updated by the law of motion (eq. (1.b), eq. (1.c)).

To reproduce correctly the behavior of the cohesive material, the moment is also transferred between two interacting elements (Plassiard et al., 2007 and Iwashita and Oda, 2000). The relative rotation angle, θ_r, was calculated, and has been put together with the rotational stiffness, k_r, the elastic moment between two elements in contact can be expressed by:

$$M_{elastic} = \sum \theta_r * k_r \qquad . \qquad (2)$$

If the actual moment is superior to the threshold of the elastic limit, then the plastic moment will take place. The plastic moment is defined by:

$$M_{plastic} = \eta * F_n * R_{avg} \quad , \qquad (3)$$

where η is the control factor of the elastic moment limit, F_n is the normal contact force and R_{avg} is the average radius of two interacting elements. Thus, an elastic-plastic behavior is involved in this law (see Fig. 1);
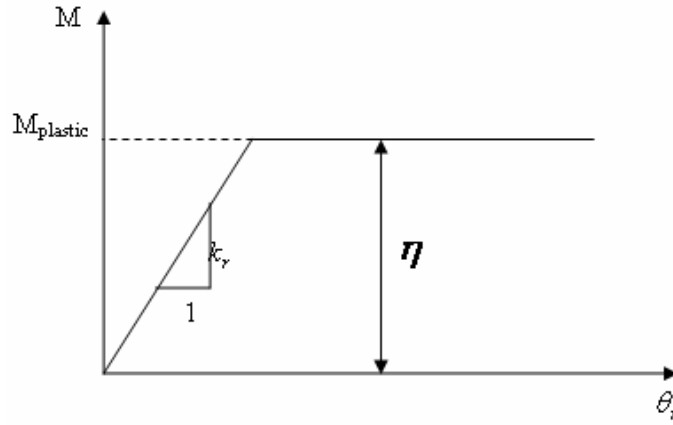
Fig 1: Evolution of the moment transfer law

Energy dissipation was also taken into account in the numerical model. The energy involved between two interacting elements is dissipated through frictional sliding for which the Coulomb internal friction angle θ_i and the cohesion C, are defined. Thus, the sliding criterion can be written as:

$$F_{s,\max} = F_n \tan\phi_i + C * S_{\text{int}} \qquad , \qquad (4)$$

where $F_{s,\max}$ is the maximum tangent force, F_n is the normal contact force and S_{int} is the average cross section of the two interacting elements. If the shear contact force exceeds $F_{s,\max}$, then the sliding mode is activated.

Moreover, a local non-viscous damping is used (Cundall and Stracks, 1979), where the damping force is put together with the equation of motion such that,

$$F_{(i)} + F_{(i)}^d = M_{(i)} A_{(i)} \qquad , \qquad (5)$$

where $F_{(i)}$, $M_{(i)}$, and $A_{(i)}$ are the generalized force, mass and acceleration components respectively, and $F_{(i)}^d$ is the damping force

6

$$F_{(i)}^d = -\alpha \left| F_{(i)} \right| sign(V_{(i)});$$

$$sign(y) = \begin{cases} +1, & \text{if } y > 0; \\ -1, & \text{if } y < 0; \\ 0, & \text{if } y = 0 \end{cases} \qquad , \qquad (6)$$

where α is the numerical damping.

2.1. The updated local constitutive law of the numerical model

Concrete can be considered as an isotropic elastic quasi-brittle material. The definition of the limit bearing capacity of concrete depends strongly on the loading situations. The proposed local constitutive law has been developed according to the experimental results obtained from high confinement triaxial tests (Gabet et al., 2007).

Fig. 2 shows the updated local constitutive law of concrete, which only concerns the normal interaction force between two discrete elements. This normal force can be split into two parts, the compressive and the tensile components. During compression, concrete first undergoes an elastic response (section AB), which is calculated by Eq. (7):

$$F_n = K_n * (D_{ij} - D_{init}) \qquad , \qquad (7)$$

where F_n is the normal contact force, K_n is the tangent stiffness, D_{ij} is the actual distance between element i and element j and D_{init} is the initial equilibrium distance. Note that $K_n = E * R_{avg}$, where E is a reference Young's Modulus and R_{avg} is the average radius of two interacting elements. Doing so, the tangent stiffness K_n depends on the size of the elements.

If the interaction distance exceeds the elastic limit distance (D_l), then the hardening plastic behavior takes place (Section BC and CD on Fig. 2), which is characterized by two successive stages. These two stages involve two different stiffness coefficient

controlled by two ratios ζ_1 and ζ_2, representing the observed response of the concrete

material at extreme loading conditions (Gabet et al., 2007). Note that, in section BC, the

unloading path follows an irreversible behavior controlled by a softer coefficient

K_{n_unload}.

The tensile part (section AE on Fig. 2) uses the same tangent module (K_n) as the

compressive section AB. After the tensile force has reached its maximum value,

$F_{t\max}$, which is calculated by

$$F_{t\max} = F_{c1} * \gamma_t \qquad ,$$ (8)

where F_{c1} is the maximum elastic compressive force and γ_t is an amplified factor to

control the value of $F_{t\max}$, a softening behavior will occur with a modified tangent

stiffness $\dfrac{K_n}{\xi}$, where ξ is the softening coefficient (See Fig. 2).

If the interaction distance exceeds the rupture distance, $D_{rupture}$, then the interaction

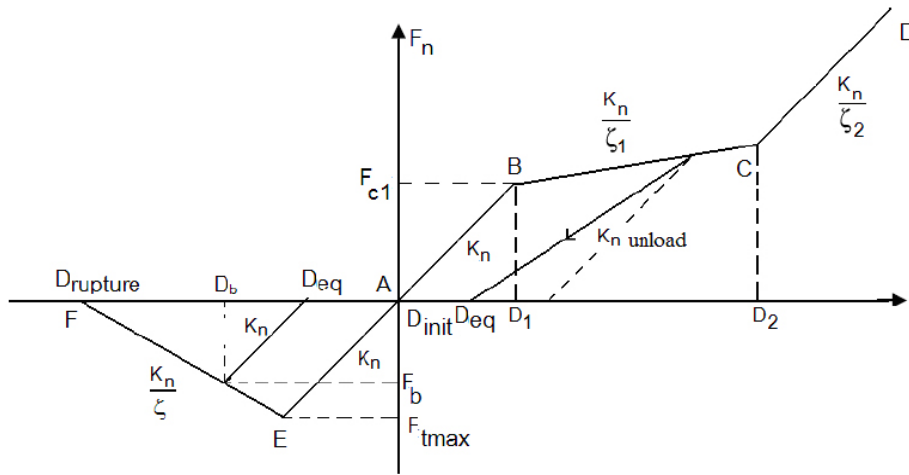force is equal to zero: the cohesive link breaks.

Fig. 2: Local normal interaction force for discrete elements representing concrete

2.2. Introducing reinforcement

A full reinforced concrete target has been simulated for the missile impact test. The steel rebar elements have been evenly placed to form a regular grid (see Fig. 3). The numerical rebars have the same diameter as the real rebars. The local interaction between the rebar's discrete elements is shown in Fig. 3. An elastic-plastic constitutive law has been used to represent the behavior of steel. The loading behavior is the same in tension and in compression, i.e the maximum elastic compressive force, $F_{cr,max}$, is equal to the maximum elastic tensile force, $F_{tr,max}$. Furthermore, a tensile breaking strength is introduced: when the distance between two rebar elements exceeds $D_{rupture}$, then the rebar breaks.
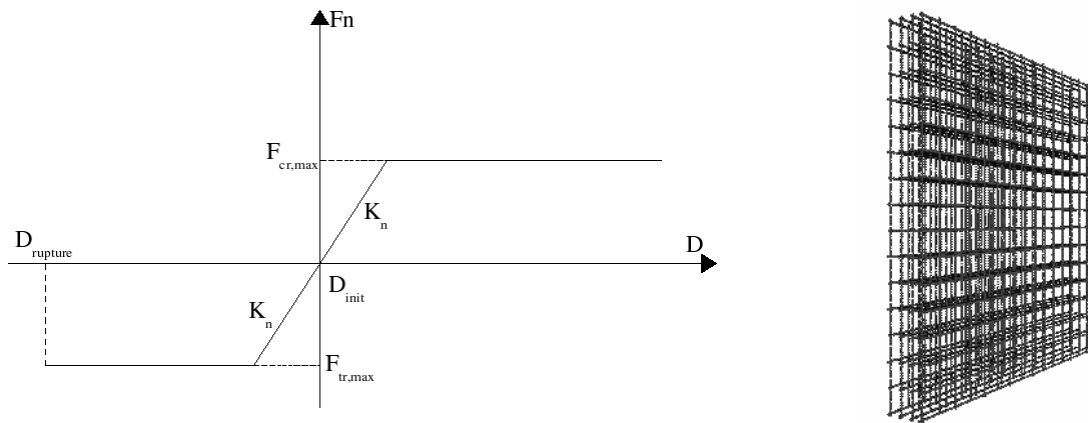

Fig. 3: Local constitutive law of the reinforcement and the spatial arrangement of the reinforcement

2.3. The model calibration process

Using the DEM approach, the impacted wall is represented by a set of discrete elements. Local constitutive parameters are assigned to each of the interaction force between the elements, such that the macroscopic behavior of the entire set is

representative of the real material at the scale of the structure. To assign the values of the local constitutive parameters, a calibration procedure, similar to previous work (Hentz et al., 2004b and Belheine et al., 2007) is used. It is based on the simulation of quasi-static uniaxial compression/traction tests. Here, a compression test model is developed in YADE for a standard-sized specimen, with the following characteristics:

  • a compact, polydisperse discrete element set is generated,

  • an elastic compression test is run with local elastic parameters given by the "macro-micro" relations (Hentz et al., 2004b),

  • compressive rupture axial tests are simulated to deduce the plastic local parameters.

Fig. 4 shows the results of the simple compression test. The numerical simulations fit well to the experimental ones. By performing these tests, the local parameters (ζ, C, θ_i,...) have been calibrated. However, performing this simple uniaxial compression test is not sufficient to obtain the full plastic response shown previously in Figure 2. It is thus necessary to calibrate the plasticity stiffness ratios ζ_1 and ζ_2, with a hydro-static test at a high confining pressure. The 650 MPa test was used as comparison. The result is shown in Fig. 4. Using the same elastic parameter as in the uniaxial compression test, the numerical result agrees well with the experimental test. The local constitutive parameters have now been fully calibrated. The parameters chosen for simulations are reported in Table 1.
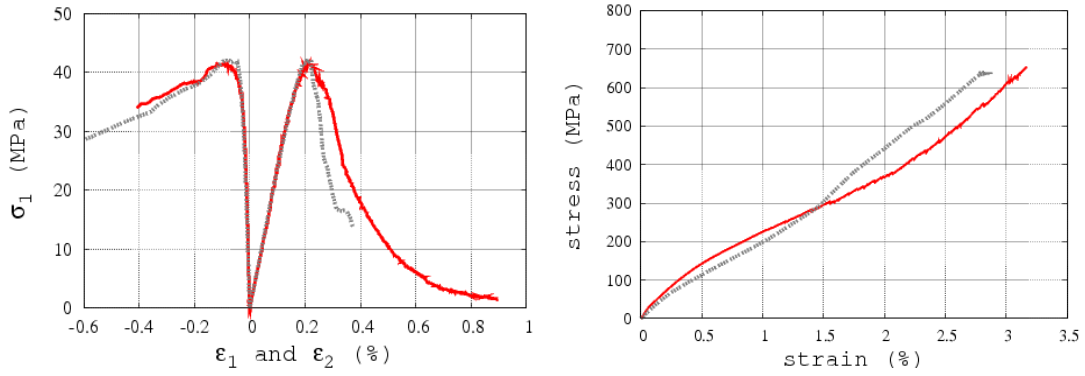
Fig. 4: Strain-stress curves of the uniaxial compression test (left) and the hydro-static test with a confinement of 650MPa (right). Solid and dashed lines are, respectively, experimental and numerical results.

Parameters	E (GPa)	C (MPa)	θ_i (degree)	ξ	γ_t	ξ_1	ξ_2
Value used	30	4	30	5	0.1	10	0.4

Table 1: Values of the local parameters

3. Modeling impact tests

3.1. Experimental test

The impact experiments were performed by the French Atomic Energy Agency (CEA) and the French Electrical power Company (EDF) on reinforced concrete slabs (Berriaud et al. 1978).

The objective of this work is to show how the local compaction appears and extends during dynamic loading. An impact reference case has been chosen for which the target size was 1.46 m x 1.46 m x 0.208 m. In this case, a flat nose missile was used, and its

11

weight was 34.5 kg, with an impact velocity of 151 m/s.

3.2. Numerical impact configuration

The total number of Discrete Elements used in the concrete slab was about 20 000, with a radius distribution size ranging from 0.005 m to 0.02 m. This resolution size was chosen based on the rebar's diameter, which imposed the minimum discrete element size. The total number of the rebar elements was 17408 and all of them had a radius of 0.005 m. The local parameters of the impact tests are kept the same as those of the static validation tests. The numerical damping factor α is set to 0.1.

The missile was simulated by a set of discrete elements which have the properties of steel. The missile was initially placed just beside the surface of the target with a given initial velocity. The impact configuration (position and orientation) has been set as close as possible to the observed experimental configuration, as shown in Fig. 5. Since in the real test case, the slab is maintained on four sides, the same configuration has been reproduced here by fixing a 10 cm layer on the same four sides of the slab.
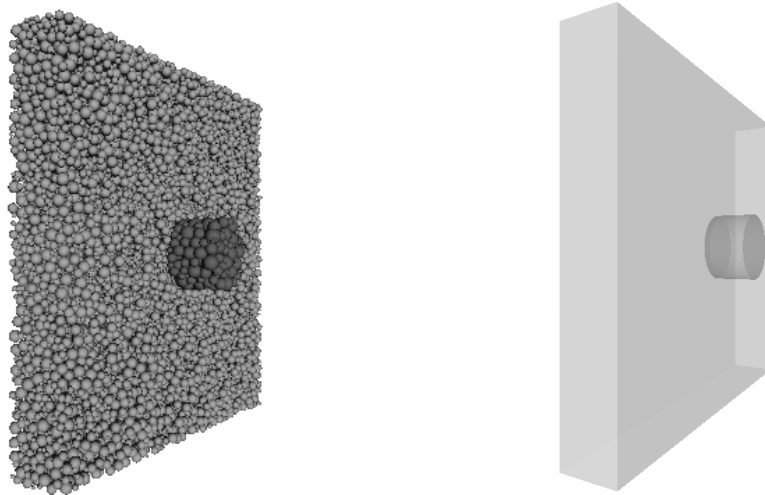

Fig. 5: On the left, the initial discrete elements configuration is represented and on the right, the outlines of this numerical model.

3.3. **Numerical results**

Recall that the reference test involves a 1.46 m x 1.46 m concrete slab with a 0.208 m thickness, reinforced by four different steel layers, impacted by a 34.5 kg non-deformable flat nose missile with a diameter of 0.278 m at velocities of 151 m/s. At this impact velocity the slab was just perforated (Fig 6).
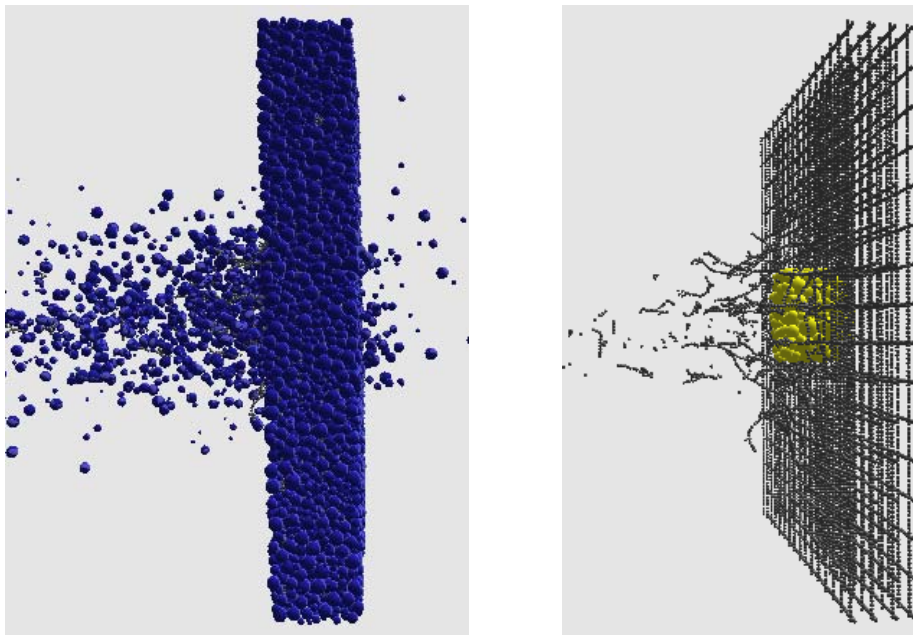

Fig. 6: Snap shot of impact reference test at t = 11 ms with impact velocity = 151 m/s.

The numerical simulation was compared not only to the experimental data obtained by the CEA and EDF, but also to a previous numerical simulation (Shiu at al., 2007a) which had been run with a commercial discrete element code (PFC^{3D}, 2003) in which only a local elastic-brittle law was implemented. The different results are shown in Fig. 7, where the target and the position of the rebars are mentioned on the vertical axis.
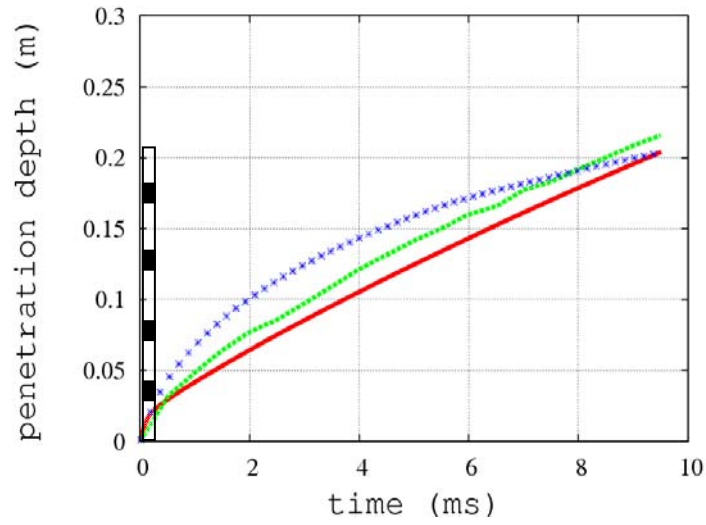
Fig. 7: Comparison of the trajectory of the missile with different local constitutive laws. Solid, dotted and starred lines are, respectively, experiments, elastic-bilinear hardening-damage constitutive law and elastic-brittle constitutive law.

Both, the elastic-brittle law obtained with PFC^{3D} and the elastic-plastic-damage law obtained with YADE predict the trajectory of the missile during its penetration in the slab. If focusing on the compaction process during the first milliseconds after impact, as displayed in the YADE code, the amount of interaction forces in the concrete slab reaching the hardening stage remains low with only 1.5% while 50% of the interactions are under tension loading (Fig 8).
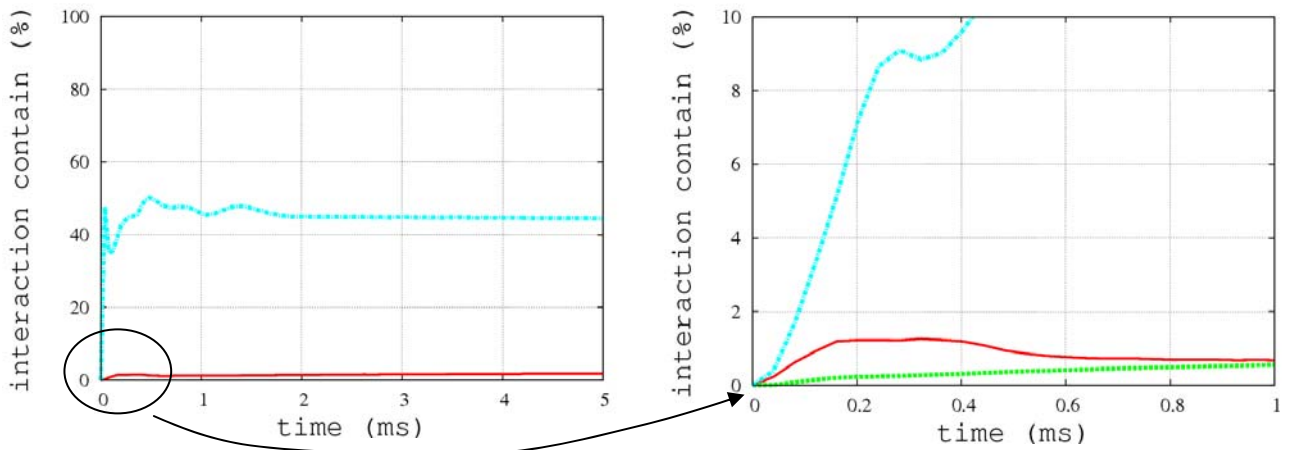
Fig. 8: On the left, the evolution of the amount of interaction forces which have reached the hardening stage (lower curves) and the tension stage (higher curve) in the concrete slab. On the right, the detailed diagram of the first ms, the lower curve corresponds to the hardening CD stage, the middle one to the hardening BC stage and the higher one to the tension stage.

Thus, for the reference case, most of the compaction involves a densification of the arrangement of the spherical discrete elements close to the impactor, whereas the amount of interaction forces reaching the hardening zone (which corresponds to higher stage of compaction) remains low.

This kind of response for an impacted concrete wall, where a low compaction process occurs, is possible when:

1. the impact velocity is low, which produces an elastic wave propagation,

2. the missile's nose is flat, which increases the amplitude of this elastic wave,

3. the thickness of the target (0.208 m) is on the same order as the missile's diameter (0.278 m), which amplifies the scabbing process.

As soon as the scabbing process takes place, the back fracturing zone reaches the one

located next to the missile creating a "tunneling" effect, which facilitates the missile progression (Shiu et al., 2007b, Magnier and Donzé, 1998).

Thus, in this case, a basic local elastic-brittle constitutive law is sufficient to predict the penetration or the perforation of a missile in a thin concrete target at low impact velocities, with, however, a slightly better prediction for the more complete constitutive law.

While keeping the same configuration test, the impact velocity is now increased from 151 m/s to 500 m/s. The new trajectory of the missile is presented in Fig. 9: the missile has now completely perforated the target.
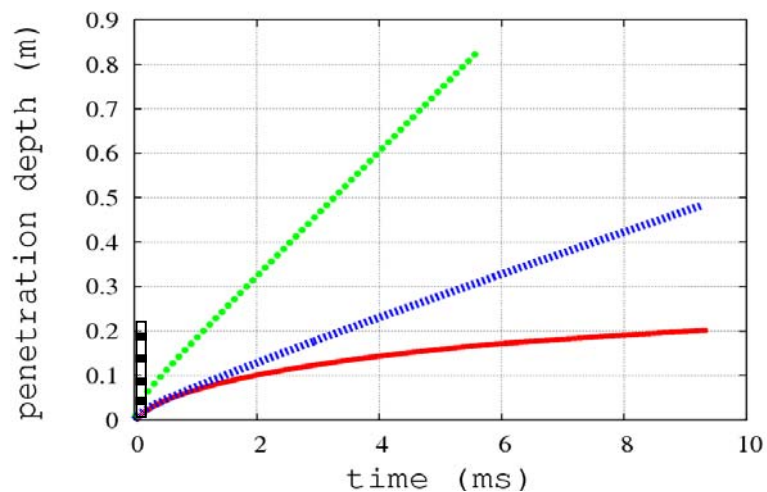

Fig. 9: Comparison of the trajectory of the missile for different impact cases. The lower, middle and upper lines are, respectively, the reference case, the case using a 16 cm wide missile with the same initial kinetic energy and the case with an impact velocity of 500 m/s.

In Fig. 10, the extension of the compacted zone inducing the hardening process at the

local scale for the two different impact velocities at t = 0.5 ms are shown. A dramatic increase of the compacted zone is observed when the impact velocity increases.

For higher impact velocities, it is observed that the back fracturing zone doesn't have enough time to reach the area located next to the missile. This induces a constant compaction process in front of the impactor and indeed, the interaction force recording data, indicates that the hardening zone has reached 7% of the interaction forces instead of the former 1.5%.
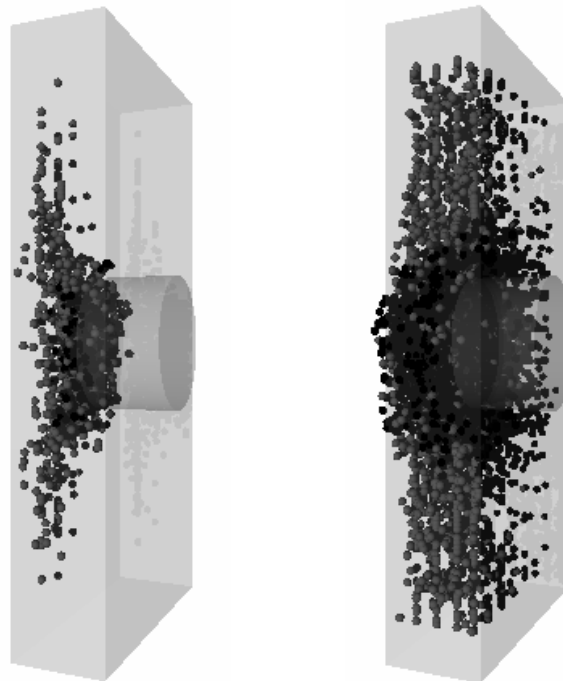

Fig. 10: Snapshots of local interaction forces in the hardening stage, at t = 0.35 ms of missile impact with v = 151 m/s , which is the reference case (left) and v = 500 m/s (right).

Another simulation was made by decreasing the missile diameter to 0.16 m, instead of

0.278 m, while keeping the same kinetic energy as in the reference case. To do so, the impact velocity was kept constant at 151 m/s, whereas the density was increased.

In this case, where the ratio between the thickness of the target and the diameter of the missile has increased, it was observed that the missile could perforate the target more easily than in the reference case (see Fig. 9) and no scabbing process occurred. Thus, the compressive elastic wave generated by this smaller impactor did not have enough energy to create tensile fractures on the back side of the target. More of the kinetic energy is spent on the local compaction process during penetration and less dissipates in wave propagation. Even though, the amount of interaction forces in the concrete slab reaching the hardening stage is comparable to the reference case (about 1.41%), the highly compacted zone remains located close to the missile (Fig. 11).
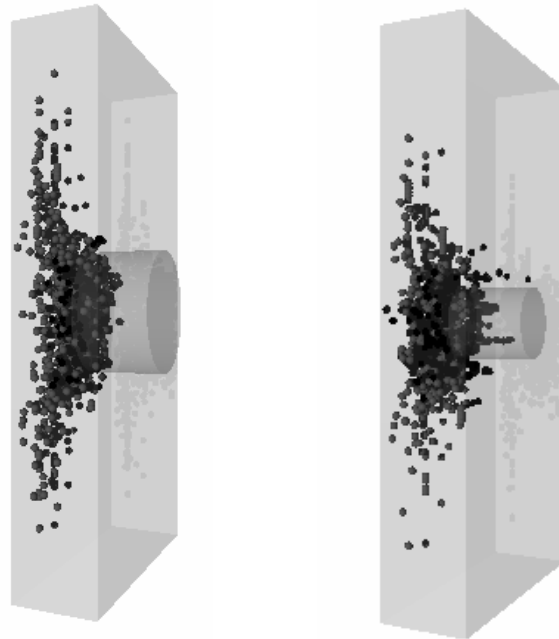

Fig. 11: Snap shots of local interaction forces in the hardening stage, at t = 0.5 ms of missile impact with v = 151 m/s , which is the reference case (left) and a missile with a diameter of 16 cm with the same initial kinetic energy (right).

4. CONCLUSION

A local elastic-bilinear hardening-damage constitutive law is developed to study the behavior of a concrete slab under extreme dynamic loading. The numerical model was constructed based on a 3D discrete element approach. The local parameters have been calibrated with a set of static tests where a simple compression test and a hydrostatic test (650 MPa) were simulated. The static simulation results agreed well with the experimental data. After finishing the validation process, the simulation of a full reinforced concrete target impacted by a rigid missile was performed. The first results show that for a thin target, both the brittle-elastic law and the elastic-bilinear hardening-damage constitutive law can well predict the penetration depth caused by the missile. In fact in the reference case, even if compaction can be seen it is nonetheless a minor part of the impact process while tensile fracturing is the major component. Thus a brittle-elastic law is sufficient to predict the response of the target in this case.

However, in order to go beyond this reference case two additional tests were then simulated. In the first one, the impact velocity was raised from 151 m/s to 500 m/s resulting in dramatically increased compacted zone, as expected. In the second one, to reduce the effect of scabbing, the ratio between the thickness of the target and the diameter of the missile was increased while keeping the kinetic energy constant. This was done by decreasing the diameter of the missile and increasing its density. This resulted in the same amount of compaction as in the reference case but differently distributed. Close to the missile head, compaction was more intense. In addition, the missile completely perforated the slab which it hadn't done in the reference case.

This work has thus provided us with a better constitutive law to use in discrete-element models for impact studies and we can now investigate impacts on thicker targets where the compaction process is important.

REFERENCES

Berriaud, C., Sokolovsky, A., Gueraud, R., Dulac, J. and Labrot, R. (1978). "Local behavior of reinforced concrete walls under missile impact", *Nuclear engineering and Design*, 45(2), 457-469.

Belheine, N., J.-P. Plassiard, F.-V. Donzé, F. Darve, A. Seridi, (2007)Numerical Simulation of Drained Triaxial Test Using 3D Discrete Element Modeling, *Computers and Geotechnics* (to appear).

Burlion, N. Gatuingt, F. Pijaudier-Cabot, G. and Daudeville, L. (2000). "Compaction and tensile damage in concrete: constitutive modelling and application to dynamics", *Computer Methods in Applied Mechanics and Engineering, 183(3-4), 291-308.*

Cundall, P.A. and Strack, O.D.L. (1979). "A discrete numerical model for granular assemblies*, Géotechnique"*, 29(1), 47-65.

Hentz S., F.V. Donzé and L.Daudeville (2004a), Discrete element modelling of concrete submitted to dynamic loading at high strain rates, Computers and Structures vol: 82 No 29-30 pp.2509-2524.

Hentz, S., Daudeville, L. and F.V. Donzé, (2004b). "Identification and validation of a discrete element model for concrete", *J. Eng. Mech*. 130(6), 709-719.

Iwashita, K. and M., Oda, M. (2000). "Micro-deformation mechanism of shear banding process based on modified distinct element method", *Powder Technology.* 109, 192-205.

Kozicki, J. and F.V Donzé (2007), "Applying an open-source software for numerical simulation using finite element or discrete modeling methods", *Computer Methods in Applied Mechanics and Engineering*, *submitted, to appear*.

Gabet T., Y., Malecot & L., Daudeville 2007. Triaxial behaviour of concrete under high stresses: influence of the loading path on compaction and limit states. *Cement & Concrete Research. (accepted, to appear)*

Magnier, S.A. & F.V. Donzé (1998), Numerical simulation of impacts using a discrete element method, Mech. Cohes.-frict. Mater. 3, 257-276.

PFC^{3D} (Particle Flow Code in 3 Dimensions), Version 3.0. (2003). Itasca Consulting Group Inc., Minneapolis, Minnesota.

Plassiard J-P, N. Belheine & F.V. Donzé (2007), Calibration Procedure for spherical discrete elements using a local moment law, *DEM 07*, Brisbane.

Shiu W., F-V., Donzé F. & L., Daudeville (2007a). "Discrete element modelling of missile impacts on a reinforced concrete target". *Int. J. Computer Applications in Technology. (to appear)*.

Shiu, W, F-V., Donzé and L. Daudeville (2007b)., Penetration prediction of missiles with different nose shapes by the discrete element approach, *Computers and Structures*, (*to appear*).

YADE, Open Source Discrete Element Code (2004), http://yade.wikia.com/wiki/Yade

LIST OF FIGURES

Fig. 1: Evolution of the moment transfer law

Fig. 2: Local normal interaction force for discrete elements representing concrete

Fig. 3: Local constitutive law of the reinforcement and the spatial arrangement of the reinforcement

Fig. 4: Strain-stress curves of the uniaxial compression test (left) and the hydro-static test with a confinement of 650MPa (right). Solid and dashed lines are, respectively, experimental and numerical results.

Fig. 5: On the left, the initial discrete elements configuration is represented and on the right, the outlines of this numerical model.

Fig. 6: Snap shot of impact reference test at t = 11 ms with impact velocity = 151 m/s.

Fig. 7: Comparison of the trajectory of the missile with different local constitutive laws. Solid, dotted and starred lines are, respectively, experiments, elastic-bilinear hardening-damage constitutive law and elastic-brittle constitutive law.

Fig. 8: On the left, the evolution of the amount of interaction forces which have reached the hardening stage (lower curves) and the tension stage (higher curve) in the concrete slab. On the right, the detailed diagram of the first ms, the lower curve corresponds to the hardening CD stage, the middle one to the hardening BC stage and the higher one to the tension stage.

Fig. 9: Comparison of the trajectory of the missile for different impact cases. The lower, middle and upper lines are, respectively, the reference case, the case using a 16 cm wide missile with the same initial kinetic energy and the case with an impact velocity of 500 m/s .

Fig. 10: Snapshots of local interaction forces in the hardening stage, at t = 0.35 ms of

missile impact with v = 151 m/s , which is the reference case (left) and   v = 500 m/s (right).

Fig. 11: Snap shots of local interaction forces in the hardening stage, at t = 0.5 ms of missile impact with v = 151 m/s , which is the reference case (left) and a missile with a diameter of 16 cm with the same initial kinetic energy (right).

List of TABLE

Table 1: Values of the local parameters